Master's Thesis
석사 학위논문

Fabrication of Ultra-Thin Photo-Multiplication Photodiode by Using a Non Fullerene-Based 2D Planar Small Molecular Semiconductor as an Efficient Optical Sensitizer

Neethipathi Deepan Kumar
Department of
Energy Science & Engineering

DGIST

2020

Master's Thesis
석사 학위논문

Fabrication of Ultra-Thin Photo-Multiplication Photodiode by Using a Non Fullerene-Based 2D Planar Small Molecular Semiconductor as an Efficient Optical Sensitizer

Neethipathi Deepan Kumar
Department of
Energy Science & Engineering

DGIST

2020

Fabrication of Ultra-Thin Photo-Multiplication Photodiode by Using a Non Fullerene-Based 2D Planar Small Molecular Semiconductor as an Efficient Optical Sensitizer

Advisor: Professor Dr. Dae Sung Chung
Co-advisor: Professor Dr. Ju Hyuck Lee

by

Neethipathi Deepan Kumar
Department of Energy Science & Engineering
DGIST

A thesis submitted to the faculty of DGIST in partial fulfillment of the requirements for the degree of Master of Science in the Department of Energy Science & Engineering. The study was conducted in accordance with the Code of Research Ethics[1]

2019. 11. 26

Approved by

Professor Dr. Dae Sung Chung (Advisor)	(signature)
Professor Dr. Ju Hyuck Lee (Co-Advisor)	(signature)

[1] Declaration of Ethical Conduct in Research**:** I, as a graduate student of DGIST, hereby declare that I have not committed any acts that may damage the credibility of my research. These include, but are not limited to: falsification, thesis written by someone else, distortion of research findings or plagiarism. I affirm that my thesis contains honest conclusions based on my own careful research under the guidance of my thesis advisor.

Fabrication of Ultra-Thin Photo-Multiplication Photodiode by Using a Non Fullerene-Based 2D Planar Small Molecular Semiconductor as an Efficient Optical Sensitizer

Neethipathi Deepan Kumar

Accepted in partial fulfillment of the requirements for the degree of Master of Science.

2019. 11. 26

	_____
Head of Committee	Prof. Dae Sung Chung (signature)
	_____
Committee Member	Prof. Ju Hyuck Lee (signature)
	_____
Committee Member	Prof. Jongmin Choi (signature)

MS/ES
201824001

Fabrication of Ultra-Thin Photo-Multiplication Photodiode by Using a Non Fullerene-Based 2D Planar Small Molecular Semiconductor as an Efficient Optical Sensitizer. Department of Energy Science & Engineering 2020.38P.Advisors Prof. Dae Sung Chung, Co-Advisors Prof. Ju Hyuck Lee

ABSTRACT

In this work, we explore the possibility of using nonfullerene and a planar n-type small molecular semiconductor, 2,2′-((2Z,2′Z)-((4,4,9,9-tetrahexyl-4,9-dihydro-s-indaceno[1,2-b:5,6-b′]dithiophene-2,7-diyl)bis(methanylylidene))bis(3-oxo-2,3-dihydro-1H-indene-2,1-diylidene))dimalononitrile (IDIC) as an optical sensitizer to improve the EQE and reduce the thickness of the photoactive layer to 70 nm. A key idea of this work is utilizing the unique photophysical properties of IDIC with an anisotropic electron transport. As is well known, contrary to spherical PCBMs (PC61BM and PC71BM) with an isotropic charge transport property, the 2D planar IDIC with an inherently anisotropic packing structure tends to hinder the formation of the effective electron percolation pathways. This is a very important requirement for the optical sensitizer of PM-OPDs because it leads to more efficient charge trapping. In addition, IDIC possesses a relatively higher absorption coefficient in the visible range compared to PC71BM, which can contribute to a higher photocurrent. Together with a deeper lowest unoccupied molecular orbital (LUMO) level of IDIC compared to PC71BM, all the mentioned photophysical properties of IDIC can be much more beneficial as optical sensitizers of the PM-OPDs. Layer-by-layer deposition of P3HT as a photoactive layer and IDIC as an optical sensitizer enables more effective PM operation, yielding high EQE exceeding 130,000% and specific detectivity over 10^{12} Jones at 150-nm-thick active layer. Furthermore, due to more facile spatial confinement of the charge carriers, the photoactive layer thickness was further decreased down to 70 nm while maintaining reasonably high EQE of 60,000% as well as specific detectivity over 10^{12} Jones. Physical origins of such synergetic effects of using IDIC as an optical sensitizer are fully discussed with various photophysical analyses in the forthcoming sections.

Keywords: Photo Multiplication, Photodetector, High Detectivity, Optical Sensitizer.

List of Contents

Abstract ····· i
List of contents ····· ii
List of figures ····· iii

1 - **Introduction** ····· 2
1.1 Introduction to PM based Photodetector ····· 2
1.2 Mechanism – Photo Multiplication Type Photodetector ····· 3
1.3 PM Type Photodetector – Advantages and Disadvantages ····· 4
1.4 Recent Trends in PM type Photodiodes ····· 5
1.5 Current Thesis Work ····· 7
2 – **Experimental Section** ····· 9
2.1 Preparations ····· 9
2.1.1 Material Preparations ····· 9
2.1.2 Device Preparations ····· 10
2.2 Characterizations ····· 11
2.2.1 Material Characterization ····· 11
2.2.2 Device Characterization ····· 14
3 – **Results and Discussions** ····· 17
4 – **Conclusions** ····· 31
References ····· 32
요 약 문 ····· 37
Acknowledgement ····· 38

Figure 1. The schematic description for planar heterojunction morphology and operating mechanism under reverse bias condition ·····3
Figure 2. Representation of this thesis work ·····7
Figure 3. Referred Synthesis route of IDIC ·····9
Figure 4. Cyclic voltammograms of IDIC, PC61BM and PC71BM. ····· 11
Figure 5. (a) Normalized absorption spectra of IDIC in solution and in film. (b) Normalized absorption spectra of pristine P3HT and layer-by-layer deposited P3HT/IDIC films. ····· 12
Figure 6. Elemental Mapping using EDX Spectroscopy ····· 12
Figure 7. Confirmation of IDIC thin layer using Elemental Mapping by EDX Spectroscopy····· 13
Figure 8. EDX spectroscopy data near Al Electrode ····· 13
Figure 9. Representation of device - thin film thickness ····· 15
Figure 10. TEM measurement for the thin film layers' thickness ····· 15
Figure 11. (a,b,c) gives the cross-sectional morphology of the active layer region and (d,e,f,g) gives the TEM image between the active layer and the electrode along with their elemental mapping in the case of nitrogen, oxygen, aluminum using EDX spectra ····· 16
Figure 12. (a) Chemical structure of IDIC (optical sensitizer) and P3HT. (b) Energy level diagram for the fabricated PM-OPD with a device architecture of ITO/PEDOT:PSS/P3HT/IDIC/Al. (c) The optical image obtained from water contact angle measurement for pristine P3HT and stacked P3HT/IDIC films. (d) The schematic description for planar heterojunction morphology and operating mechanism under reverse bias condition.....18
Figure 13. (a,b) J-V characteristics of P3HT/IDIC based PM-OPD under (a) dark and (b) light illumination (Power = 0.7419 mW/cm2, wavelength = 450 nm) at various temperatures in the forward bias regions. (c,d) Experimentally obtained ln (J0T−2) versus 1000/T plot under (c) dark and (d) illumination condition to calculate the Schottky barrier height. ····· 21
Figure 14. J-V characteristics of P3HT/PC71BM based PM-OPD under (a) dark and (b) light illumination (Power = 0.7419 mW/cm2, wavelength = 445 nm) at various temperatures in the forward bias regions. (c) Experimentally obtained ln (JsT−2) versus 1000/T plot under both dark and illuminated conditions to calculate the Schottky barrier height. ····· 23
Figure 15. (a) J-V characteristics of PM-OPD with a 150-nm-thick active layer under dark and illuminated conditions (wavelength of 450 nm and power intensity of 44.7 μW/cm2), (b) EQE spectrum with a maximum of 130,000% measured at 19 V under reverse bias, (c) noise current spectrum measured at 10 V under reverse bias, and (d) the corresponding specific detectivity spectrum.. ····· 25
Figure 16. (a) J-V characteristics of PM-OPD with a 70-nm-thick active layer under dark and illuminated conditions (wavelength of 450 nm and power intensity of 39.81 μW/cm2), (b) EQE spectrum with a maximum of 60,700% measured at 19 V under reverse bias, (d) LDR range ····· 27
Figure 17. Comparison of Gain obtained by various thick active layer at -19 V····· 28
Figure 18. Comparison of EQE obtained by the 150nm thick photodetector under different reverse bias condition ····· 29
Figure 19. Maximum Gain obtained at different active layer thickness ····· 29
Figure 20. Theoretical Gain Vs Experimental Gain ····· 30
Table 1. Reported Literatures of P3HT based PM-OPDs ·····6
Table 2. Thickness Vs Maximum EQE obtained ····· 30

Fabrication of Ultra-Thin Photo-Multiplication Photodiode by Using a Non Fullerene-Based 2D Planar Small Molecular Semiconductor as an Efficient Optical Sensitizer

1. INTRODUCTION

1.1 Introduction to PM based Photodetector:

Image sensors are emerging as a core technology for industrial robots, precision inspection equipment, autonomous vehicles, and drones with the advent of the fourth industrial revolution, and their application areas are continuously increasing.[1] A key component of an image sensor is a photodiode that converts an optical signal into an electrical signal, typically a Si photodiode. Although Si has been successfully used as a photoactive layer in image sensors for decades, it has a poor integrity. Si has a low absorption coefficient due to its indirect bandgap, which requires the thickness of the photoactive layer to be in the micrometer range.[2] Owing to this, there is a clear limitation in further enhancing the resolution of Si based complementary metal–oxide–semiconductor image sensors (Si-CMOS).

Panasonic's recent products demonstrated that the size of pixels in photodiodes can be significantly reduced using organic semiconductors with decreased thickness of the photoactive layer.[3] As revealed by many earlier studies on organic photodiodes (OPDs) with high detectivity of over 10^{12} Jones, a higher absorption coefficient of organic semiconductors (compared to Si) enables thinner active layers, with thicknesses as less as several hundred nanometers.[4-7] Ironically, one of the drawbacks of the OPDs developed so far is their thickness. Typically, organic semiconductors have sufficiently high absorption coefficient; hence, only ~100 nm thickness is adequate to fully absorb most visible light.

Nonetheless, most high-performance OPDs currently in use—including Panasonic's prototype product—use photoactive layer thicknesses around ~500 nm, which is required to improve the OPD performance as a sensor, i.e., to improve the signal-to-noise ratio.

Earlier research works on OPDs showed that ~500 nm thickness is optimal for minimized dark/noise current without seriously sacrificing photocurrent. Although 500 nm is far thinner than the 3-μm thickness of the Si photodiode, development of much thinner OPD is desirable, as this further accelerates overall degree-of-integration of organic image sensors. In this context, the photo-multiplication (PM)-type organic photodetector has been actively studied recently

1.2 Mechanism – Photo Multiplication Type Photodetector

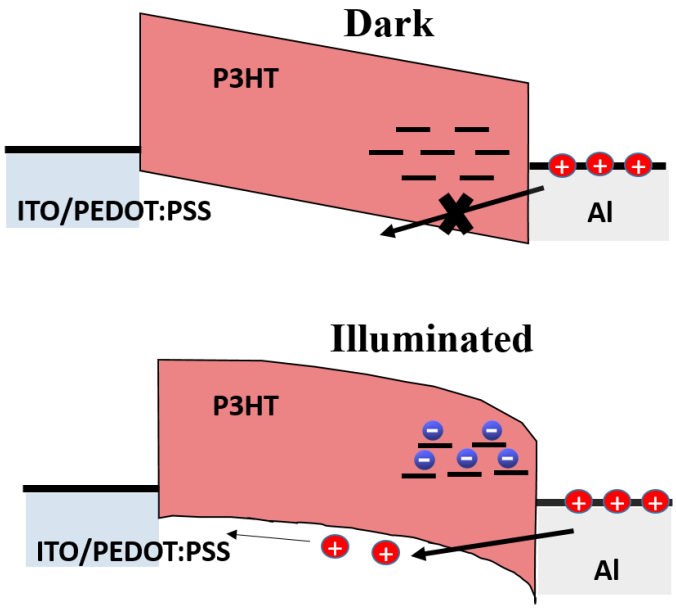

Figure 1. The schematic description for planar heterojunction morphology and operating mechanism under reverse bias condition

Basically, the PM photodetector has the same device structure as the OPD, but a significantly different principle of operation. It has a small amount of optical sensitizers acting as a charge separation and charge trapping center. Typically, optical sensitizers separate and trap photo-generated electrons from the p-type semiconductor employed as a photoactive layer. This generates the localized electric field by the trapped electrons to accelerate the injection of holes via tunneling through the Schottky barrier, which originally cannot be overcome under dark condition.[11] Because the injected holes can generate photoconductive gain by this strategy, it is called the PM photodetector. In other words, the PM photodetector is a gain-generating photoconductor whose junction nature is autonomously converted by the optical sensitizer from Schottky to Ohmic junctions

1.3 PM Type Photodetector – Advantages & Disadvantages:

One distinct advantage of the PM photodetectors is that they are relatively free from thickness issues compared to the conventional OPDs. Though the PM photodetector has a large dark current with a thin photoactive layer, the photocurrent can also be increased simultaneously via the photo-multiplication mechanism, which leads to high detectivity even with a smaller thickness. There have been intensive research efforts to realize PM-type organic photodetectors (PM-OPDs).

1.4 Recent trends in PM type based Photodiodes:

Earlier research works on OPDs showed that ~500 nm thickness is optimal for minimized dark/noise current without seriously sacrificing photocurrent. Although 500 nm is far thinner than the 3-μm thickness of the Si photodiode, development of much thinner OPD is desirable, as this further accelerates overall degree-of-integration of organic image sensors. In this context, the photo-multiplication (PM)-type organic photodetector has been actively studied recently. [8-10]

For example, *L. Li* et al. reported 37,500% of external quantum efficiency (EQE) based on poly(3-hexylthiophene-2,5-diyl) (P3HT) as a photoactive layer and [6,6]-phenyl-C_{61}-butyric acid methyl ester ($PC_{61}BM$) (200:1, w/w) as an optical sensitizer with bulk heterojunction (BHJ) geometry.[8] *W. Wang* et al. reported 53,600% of EQE based on P3HT as a photoactive layer and [6,6]-phenyl-C_{71}-butyric acid methyl ester ($PC_{71}BM$) (100:1, w/w) as an optical sensitizer by sequential stacking.[9] So far, 120,700 % of EQE reported by *M. S. Jang* et al., is the highest value, which was enabled by sequential deposition of P3HT and $PC_{71}BM$ in the layer-by-layer stacking method, leading to more efficient quenching of electron percolation.[10] Another interesting approach for such PM-OPDs is realizing charge narrow injection.[13-14] In these reports, tunable spectral responses were smartly demonstrated by changing either illumination direction or bias polarity.

~Thickness(nm)	Active Layer	~ EQE(%)	λ (nm)	Max.Detectivity	Ref
255	P3HT:PC61BM:CdTe Nanoparticles	~8000	350-700	-	1
80	P3HT:PC61BM,Ir-125	~7000	300-1050	-	2
200-300	PbS:P3HT:PC61BM:ZnO	~1600	320-1000	1.01*10^12	3
Thick Graphene layer along with 103nm of P3HT	P3HT:PC61BM: Graphene	100000	325	-	4
500	P3HT:ZnO	340000	300-650	2.5*10^14	5
80	P3HT:PC61BM: Ir125	7000	300-1050	-	6
200	P3HT:$PC_{71}BM$(100:1)/LiF	16700	300-700		7
280-300	P3HT:PTB7-Th:$PC_{71}BM$ (50:50:1)	38000	300-800	3.39*10^13	8
250	P3HT:ITIC (100:1)	5750	300-790	8.27*10^12	9
1500	P3HT:$PC_{61}BM$:CdTe (thick)	200	660	7.3*10^11	10
300	P3HT:$PC_{71}BM$ (100:1, thick)	53500	650	1.3*10^11	11
3000	P3HT:PTB7-Th:$PC_{61}BM$ (40:60:1, thick)	600	350-800	2.9*10^10	12
150	P3HT:$PC_{71}BM$(100:1) Sequential deposition	127000	300-700	1.3*10^12	13
150 70	P3HT:IDIC	130000 60000	300-700	6*10^12 4*10^12	(Current work)

Table 1. Reported Literatures of P3HT based PM-OPDs

1.5 Current Thesis work:

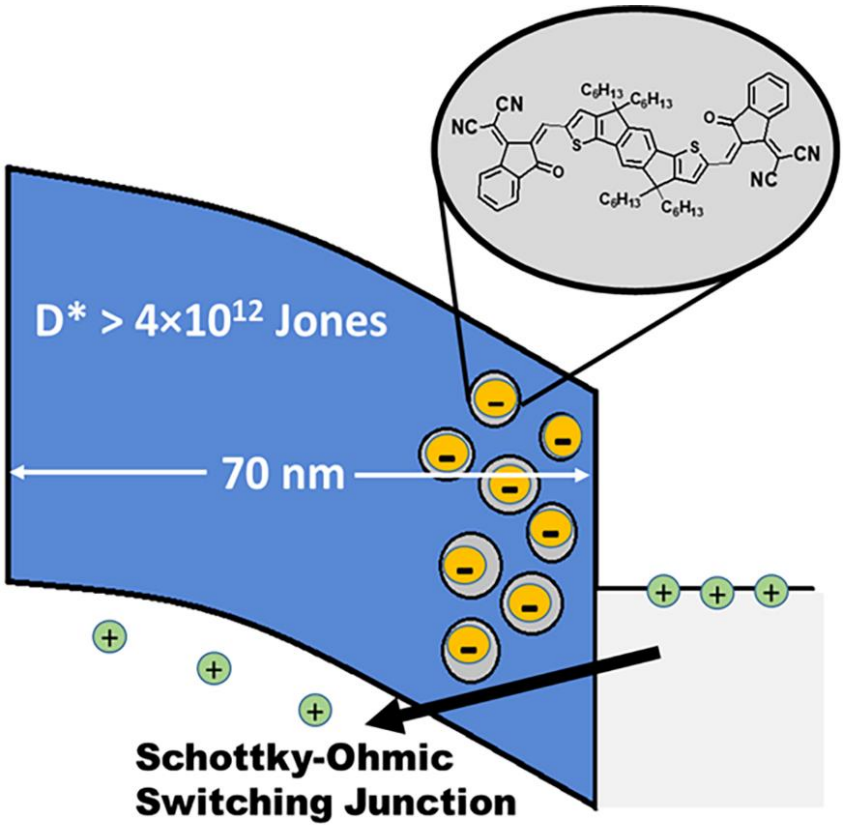

Figure 2. Representation of this thesis work

In this work, we explore the possibility of using nonfullerene and a planar n-type small molecular semiconductor, 2,2′-((2Z,2′Z)-((4,4,9,9-tetrahexyl-4,9-dihydro-s-indaceno[1,2-b:5,6-b′]dithiophene-2,7-diyl)bis(methanylylidene))bis(3-oxo-2,3-dihydro-1H-indene-2,1-diylidene))dimalononitrile (IDIC) as an optical sensitizer to improve the EQE and reduce the thickness of the photoactive layer to 70 nm. A key idea of this work is utilizing the unique photophysical properties of IDIC with an anisotropic electron transport. As is well known,

contrary to spherical PCBMs (PC61BM and PC71BM) with an isotropic charge transport property, the 2D planar IDIC with an inherently anisotropic packing structure tends to hinder the formation of the effective electron percolation pathways.[12] This is a very important requirement for the optical sensitizer of PM-OPDs because it leads to more efficient charge trapping. In addition, IDIC possesses a relatively higher absorption coefficient in the visible range compared to PC71BM, which can contribute to a higher photocurrent. Together with a deeper lowest unoccupied molecular orbital (LUMO) level of IDIC compared to PC71BM, all the mentioned photophysical properties of IDIC can be much more beneficial as optical sensitizers of the PM-OPDs. Layer-by-layer deposition of P3HT as a photoactive layer and IDIC as an optical sensitizer enables more effective PM operation, yielding high EQE exceeding 130,000% and specific detectivity over 1012 Jones at 150-nm-thick active layer. Furthermore, due to more facile spatial confinement of the charge carriers, the photoactive layer thickness was further decreased down to 70 nm while maintaining reasonably high EQE of 60,000% as well as specific detectivity over 10^{12} Jones. Physical origins of such synergetic effects of using IDIC as an optical sensitizer are fully discussed with various photophysical analyses in the forthcoming sections.

2. EXPERIMENTAL SECTION

2.1 Preparation:

2.1.1 Material Preparation:

Poly(3-hexylthiophene-2,5-diyl) (P3HT) was purchased from RIEKE METALS and [6,6]-phenyl-C71-butyric acid methyl ester (PC71BM) was purchased from Nano-C. Both the materials were used without further purification.

Synthesis of IC-C6IDT-IC:

To a three-necked round bottom flask were added C6IDT-2CHO (131 mg, 0.20 mmol), INCN (200 mg, 1.00 mmol), pyridine (1 mL) and chloroform (30 mL). The mixture was deoxygenated with nitrogen for 30 min and then refluxed for 12 h. After cooling to room temperature, the mixture was poured into methanol (200 mL) and filtered. The residue was purified by column chromatography on silica gel using petroleum ether/dichloromethane (1:1) as eluent yielding a purple solid (173 mg, 85%)

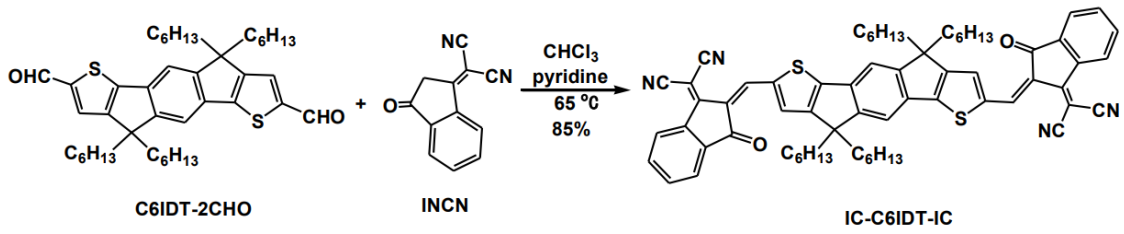

Scheme S1. Synthesis route to IC-C6IDT-IC.

Figure 3. Referred Synthesis route of IDIC

2.1.2 Device Preparations:

ITO-patterned glasses (Sheet resistance of ≈15 Ω/sq) were cleaned through sequential sonications in Mucasol solution, deionized water, acetone, and isopropyl alcohol (IPA). The cleaned substrates were then dried in a nitrogen-filled glove box and treated by O2-plasma for 5 min for further cleaning. Poly(3,4-ethylenedioxythiophene): poly(styrene sulfonate) (PEDOT:PSS) was spin-coated on top of the ITO-patterned substrate at 4000 rpm to form a thin hole transport layer, followed by baking at 120°C for 10 min. The P3HT and IDIC solutions were prepared separately.

The P3HT solutions with different concentrations (30 and 20 mg mL-1 in 1,2-dichlorobenzene) and IDIC solutions with (0.25 mg mL-1 in dichloromethane) were prepared separately for sequential deposition. The prepared P3HT solution was spin-coated onto the PEDOT: PSS-coated substrate at 800 rpm for 30 s and was dried in nitrogen-flow for 5 min. The prepared IDIC solutions were spin-coated on top of the P3HT layer at 4000 rpm for 30 s, which was thermally annealed at 70°C inside a nitrogen-filled glove box. Al electrodes were deposited onto the active layer using thermal evaporation under high vacuum (<5 × 10−6 mbar). For all devices, the resulting active layer area was 0.09 cm2.

2.2 CHARACTERIZATION:

2.2.1 Material Characterization:

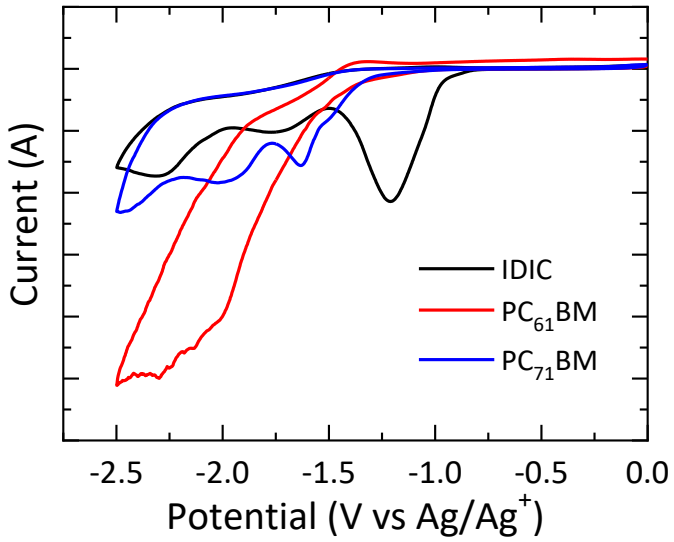

Figure 4. Cyclic voltammograms of IDIC, $PC_{61}BM$ and $PC_{71}BM$.

- Cyclic voltammograms for the small molecule IDIC and PCBM were measured, in order to calculate the HOMO and LUMO energy level.
- Later UV – Vis absorption measurements were conducted on both pristine and solution processed thin film layer IDIC, to compare their absorption spectra.
- Later Elemental mapping were conducted using two methods 1) TEM Method, 2) XPS by layer by layer etching process. The main objective of these elemental mapping is to prove the presence of 70 nm thin IDIC layer.

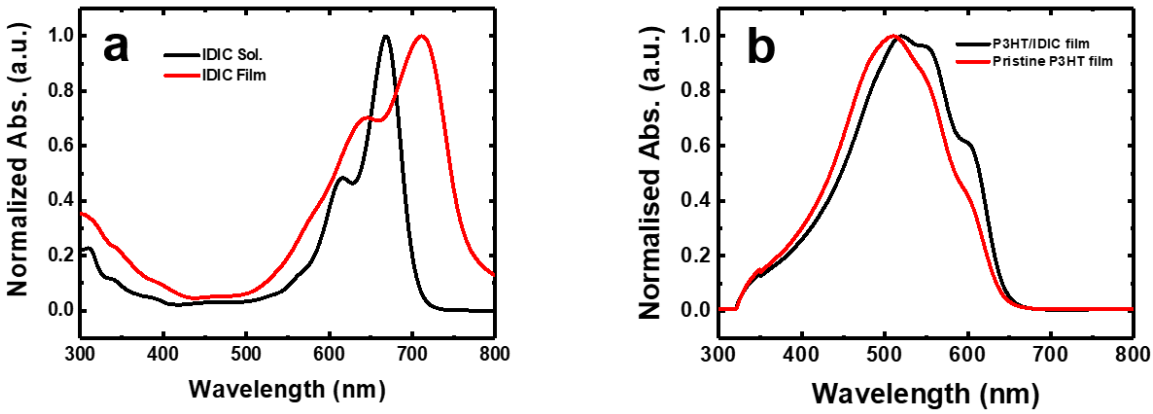

Figure 5. (a) Normalized absorption spectra of IDIC in solution and in film. (b) Normalized absorption spectra of pristine P3HT and layer-by-layer deposited P3HT/IDIC films.

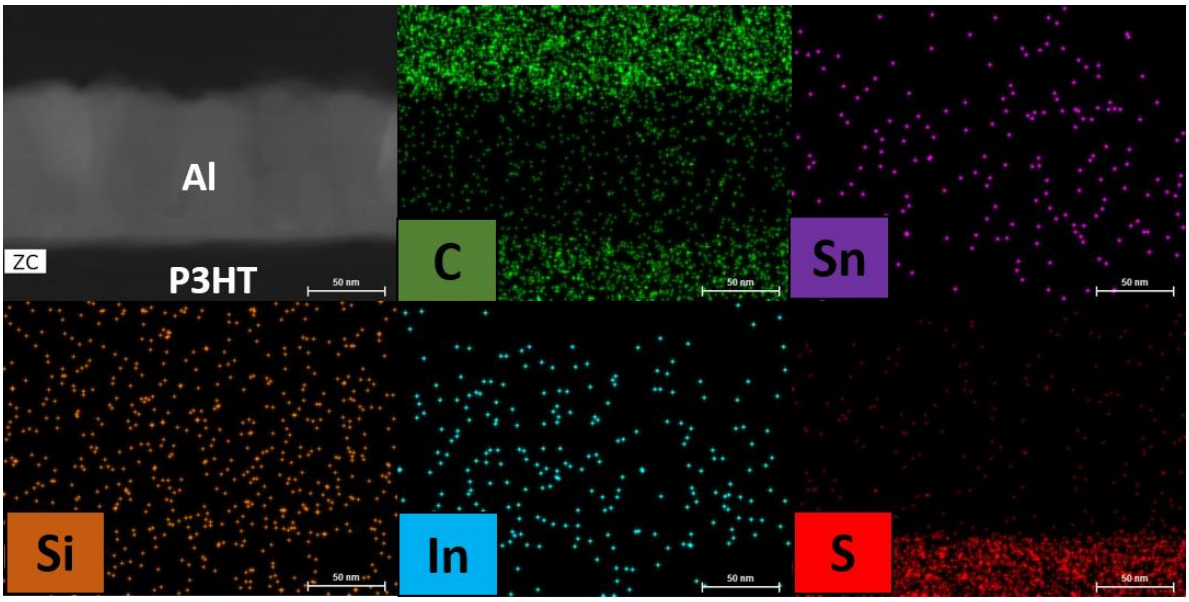

Figure 6. Elemental Mapping using EDX Spectroscopy

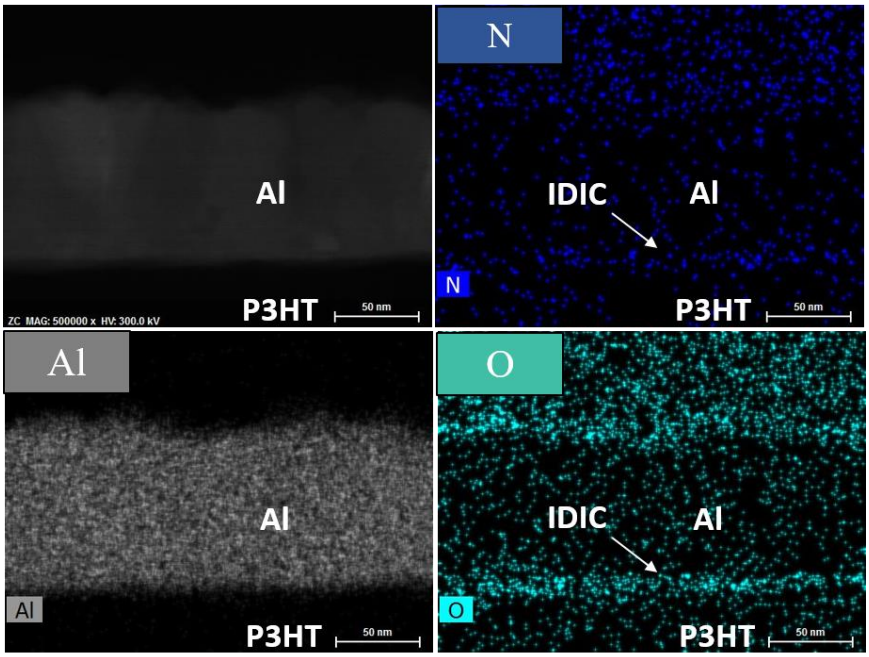

Figure 7. Confirmation of IDIC thin layer using Elemental Mapping by EDX Spectroscopy

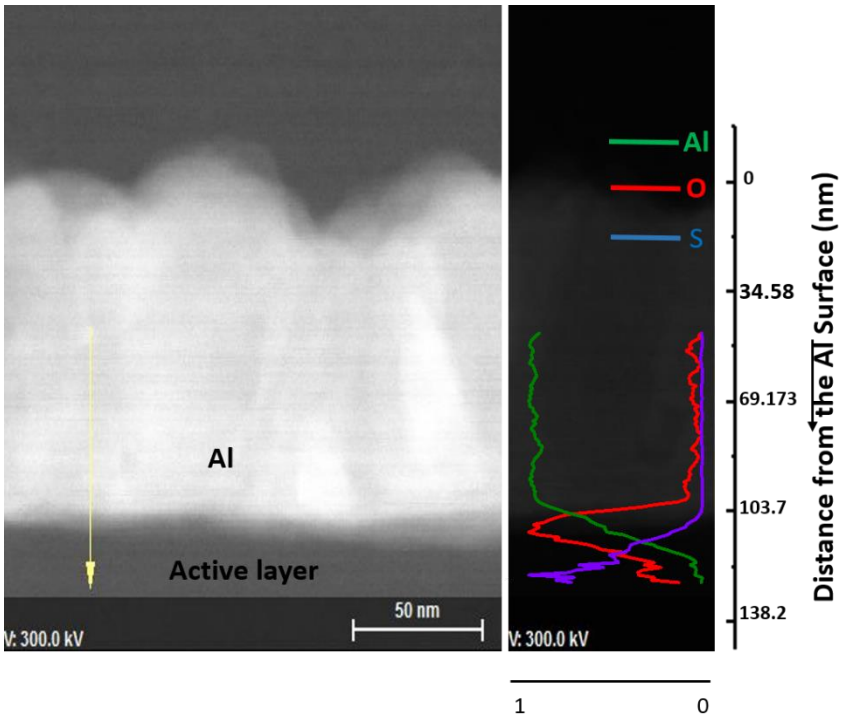

Figure 8. EDX spectroscopy data near Al Electrode

2.2.2 Device Characterization:

- The active layer thickness of different devices was measured with Surface profiler (Dektak XT).
- The J-V characteristics were measured with a Keithley 2450 sourcemeter, together with an Oriel Cornerstone 130 1/8m monochromator with the sourcemeter for measuring the photocurrent.
- The linear dynamic range (LDR) was measured with two different light sources: A monochromatic light from a 150 W xenon arc lamp dispersed from the monochromator for a light intensity below 50 μW cm−2 and a laser diode (473 nm) modulated by AFG310 arbitrary function generator (Tektronix) was used for a light intensity up to 0.7419 mW/cm2.
- Noise currents were directly measured from Stanford Research SR830 Lock-in Amplifier and were normalized by the input bandwidth.
- All the measurements regarding the photovoltaic characteristics and the stability of the device were carried out in a nitrogen-filled glovebox.

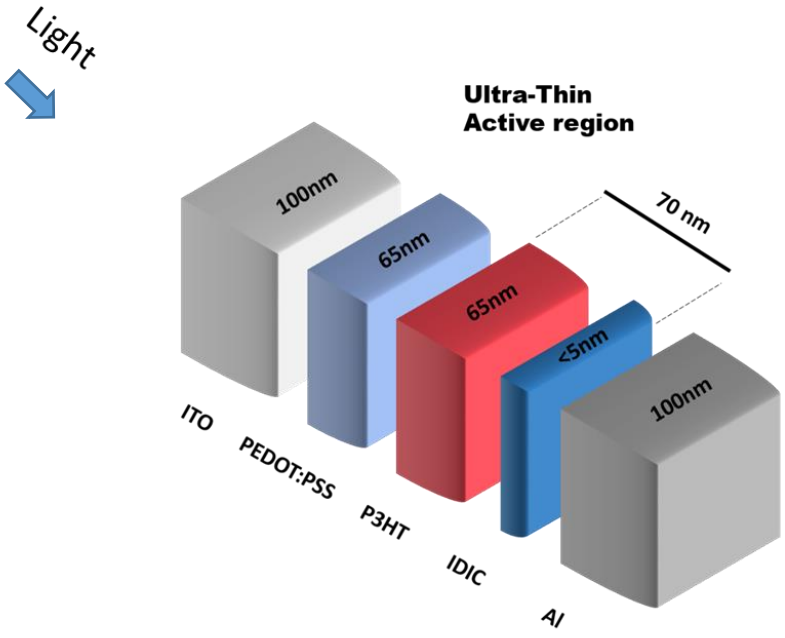

Figure 9. Representation of device - thin film thickness

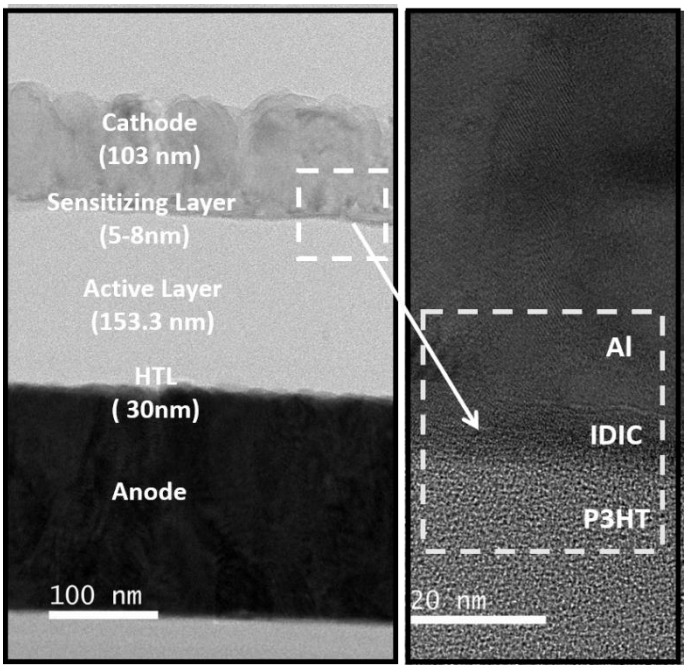

Figure 10. TEM measurement for the thin film layers thickness

TEM measurements can be successfully used to the presence of ultra-thin IDIC layer in between the cathode and P3HT layer.

This layer can be easily varied by conducting elemental mapping technique. Here the thickness varies between 5 to 8 nm thin film and the layer of P3HT was measured to be 70 nm.

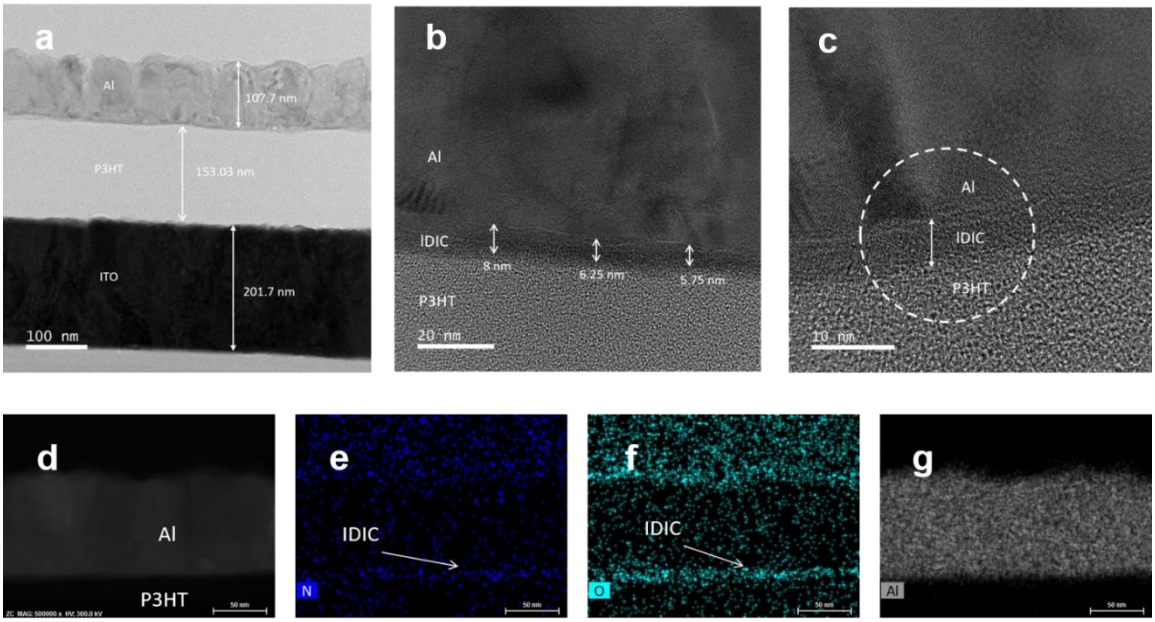

Figure 11. (a,b,c) gives the cross-sectional morphology of the active layer region and (d,e,f,g) gives the TEM image between the active layer and the electrode along with their elemental mapping in the case of nitrogen, oxygen, aluminum using EDX spectra

3. Results and discussion

In this work, we explore the possibility of using nonfullerene and a planar n-type small molecular semiconductor, 2,2′-((2Z,2′Z)-((4,4,9,9-tetrahexyl-4,9-dihydro-s-indaceno[1,2-b:5,6-b′]dithiophene-2,7-diyl)bis(methanylylidene))bis(3-oxo-2,3-dihydro-1H-indene-2,1-diylidene))dimalononitrile (IDIC) as an optical sensitizer to improve the EQE and reduce the thickness of the photoactive layer to 70 nm. A key idea of this work is utilizing the unique photophysical properties of IDIC with an anisotropic electron transport. As is well known, contrary to spherical PCBMs ($PC_{61}BM$ and $PC_{71}BM$) with an isotropic charge transport property, the 2D planar IDIC with an inherently anisotropic packing structure tends to hinder the formation of the effective electron percolation pathways.[12]

This is a very important requirement for the optical sensitizer of PM-OPDs because it leads to more efficient charge trapping. In addition, IDIC possesses a relatively higher absorption coefficient in the visible range compared to $PC_{71}BM$, which can contribute to a higher photocurrent. Together with a deeper lowest unoccupied molecular orbital (LUMO) level of IDIC compared to $PC_{71}BM$, all the mentioned photophysical properties of IDIC can be much more beneficial as optical sensitizers of the PM-OPDs. Layer-by-layer deposition of P3HT as a photoactive layer and IDIC as an optical sensitizer enables more effective PM operation, yielding high EQE exceeding 130,000% and specific detectivity over 10^{12} Jones at 150-nm-thick active layer.

Furthermore, due to more facile spatial confinement of the charge carriers, the

photoactive layer thickness was further decreased down to 70 nm while maintaining reasonably high EQE of 60,000% as well as specific detectivity over 10^{12} Jones. Physical origins of such synergetic effects of using IDIC as an optical sensitizer are fully discussed with various photophysical analyses in the forthcoming sections.

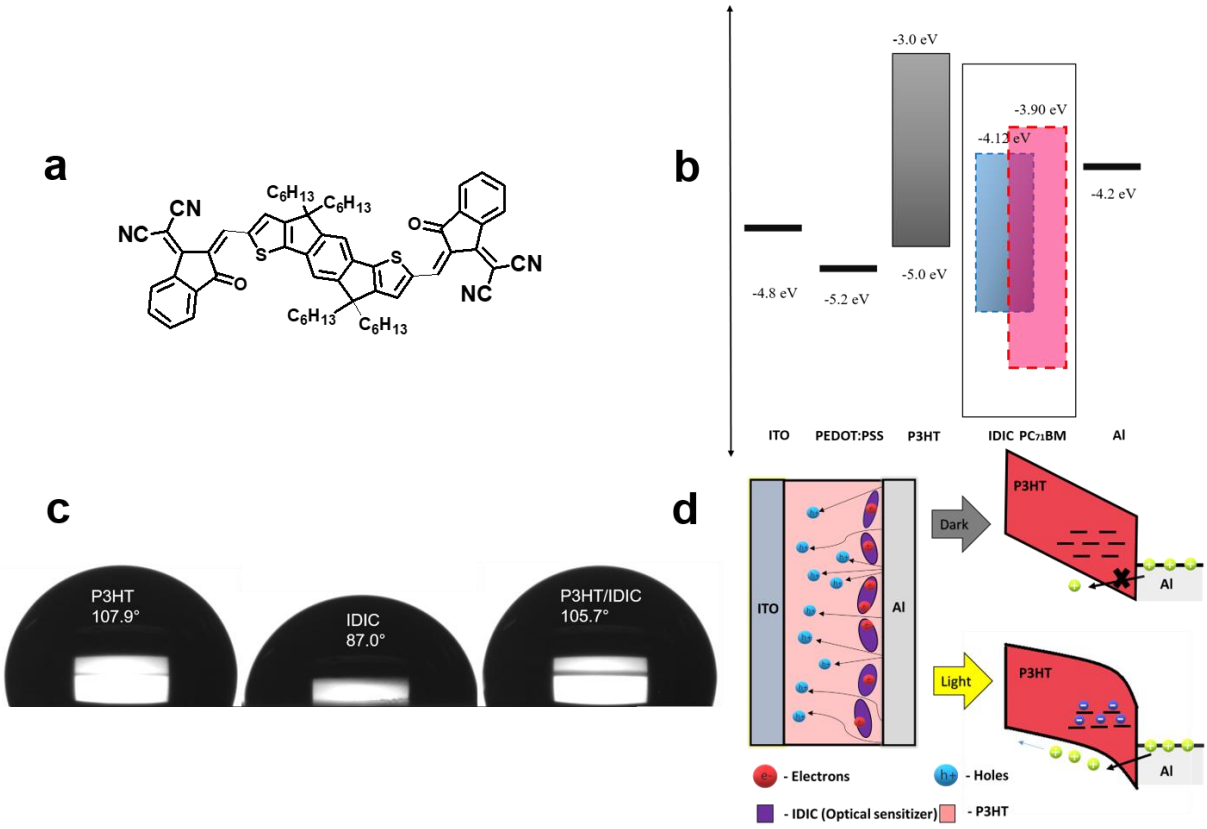

Figure 12. (a) Chemical structure of IDIC (optical sensitizer) and P3HT. (b) Energy level diagram for the fabricated PM-OPD with a device architecture of ITO/PEDOT:PSS/P3HT/IDIC/Al. (c) The optical image obtained from water contact angle measurement for pristine P3HT and stacked P3HT/IDIC films. (d) The schematic description for planar heterojunction morphology and operating mechanism under reverse bias condition.

Figure 12. (a) Chemical structure of the optical sensitizer, IDIC. (b) Energy level diagram for the fabricated PM-OPD with a device architecture of ITO/PEDOT:PSS/P3HT/IDIC/Al. (c) The optical image obtained from water contact angle measurement for pristine P3HT and stacked P3HT/IDIC films. (d) The schematic description for planar heterojunction morphology and operating mechanism. (spheres describing hole should be unified between left and right figures)

Figure 1(a) shows the chemical structure of IDIC. The energy level alignment of the suggested PM-OPD structure is schematically depicted in Figure 1(b).

The figure of merit of PM-OPD is the photoconductive gain, which is given by $gain = \tau \times t_{tr}^{-1}$, where τ and t_{tr} are the carrier lifetime and transit time, respectively.[8,13,14]

In such a photoconductive device architecture, the carrier lifetime in trap states (in this case, optical sensitizer) is determined mainly by the energy offset between the LUMO levels of P3HT and optical sensitizer, regardless of it being IDIC or PCBM. Therefore, a slightly deeper LUMO level of IDIC (-4.12 eV) compared to $PC_{71}BM$ (-3.91 eV) can accelerate the gain generation mechanism because IDIC can lead to more efficient charge separation and trapping of photo-generated electrons as optical sensitizers. The energy level for LUMO in the case of IDIC, $PC_{61}BM$ and $PC_{71}BM$ were experimentally found and were summarized by CV method.

In addition to the energy levels at which electrons can be trapped, it is also very important to induce the morphology in which the IDIC is spatially confined discretely. This enables the electron percolation pathway to be blocked. To achieve such spatially isolated IDIC domains at the interface between P3HT and Al, we employed sequential deposition of P3HT

and IDIC onto the PEDOT:PSS/ITO substrate by using orthogonal solvents of 1,2-dichlorobenzene and dichloromethane, respectively.

After layer-by-layer stacking of P3HT and IDIC followed by thermal annealing, the water surface contact angles were compared, as shown in Figure 1(c). Only typical water contact angles of the P3HT surface were observed for both pristine P3HT and P3HT/IDIC cases, while the surface of IDIC was more hydrophilic, implying that most of the IDIC molecules diffused slightly into the P3HT layer after thermal annealing.

A similar phenomenon was observed earlier in our previous work where $PC_{71}BM$ was used as an optical sensitizer of PM-OPDs.[10] Hence, we can assume spatially confined morphology of IDIC within the P3HT matrix near Al electrode. The overall morphological features are schematically depicted in Figure 1(d) with a simple description on the operating mechanism of the PM-OPD. The absorption spectra are shown in Figure.

A key idea of this work is employing IDIC instead of PCBM for more efficient gain generation of the PM-OPDs. The suggested PM-OPD is basically a gain-generating photoconductor, in which the P3HT/Al junction is promptly converted from the Schottky junction to Ohmic junction under illumination with the assistance of optical sensitizer; hence, comparing effective barrier height for hole injection with IDIC or $PC_{71}BM$ sensitizers would be the most direct method to judge the overall out-performing of IDIC compared to that of $PC_{71}BM$.

The ideal diode equation can be expressed as

$$J = J_s \left[\exp\left(\frac{q(V)}{kT}\right) - 1\right] - J_{ph}$$

where J_s is the dark saturation current density, V is the applied voltage, k is the Boltzmann's constant, T is the temperature, and J_{ph} is the photocurrent density.[15]

When forward bias is sufficiently high, this equation can be simplified to approximately $J = J_s\left[\exp\left(\frac{q(V)}{kT}\right)\right]$, from which we can obtain the temperature-dependent J_s plot.

Assuming that the Boltzmann-type energetic uphill injection in the PM-OPD follows the thermionic emission theory, as is widely accepted for the Schottky barrier injection, the temperature dependence of J_s can be theoretically described as

$$J_s = A^* T^2 exp(\frac{-\varphi_B}{kT})$$

where A^* is the Richardson constant and φ_B is the effective barrier height.[16]

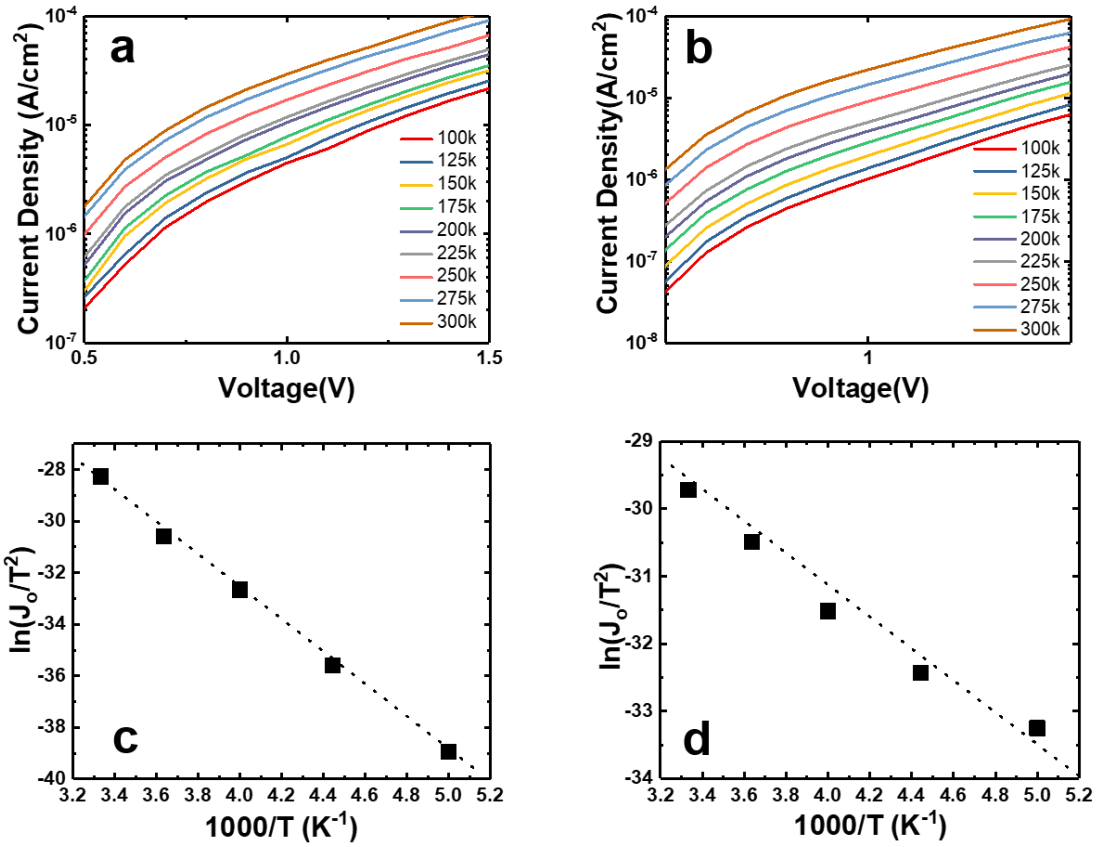

Figure 13. (a,b) J-V characteristics of P3HT/IDIC based PM-OPD under (a) dark and (b) light illumination (Power = 0.7419 mW/cm2, wavelength = 450 nm) at various temperatures in the forward bias regions. (c,d) Experimentally obtained ln (J0T−2) versus 1000/T plot under (c) dark and (d) illumination condition to calculate the Schottky barrier height.

Therefore, the slope of $\ln(J_sT^{-2})$ versus $(1/T)$ plot can provide φ_B. Figures 2(a) and 2(b) summarize the dark and illuminated (light intensity =0.7416 mW/cm^2, wavelength = 450 nm) *J-V* characteristics of IDIC-based PM-OPD, respectively. Figures 13(c) and 13(d) show the corresponding $\ln(J_sT^{-2})$ versus $(1/T)$ plot for dark and illuminated conditions, respectively.

The extracted effective Schottky barrier heights for the dark and illuminated conditions were 0.55 and 0.185 eV, respectively, implying that the PM-OPD can have Ohmic-like junction at the P3HT/Al under illumination as well as Schottky junction under dark. This is in good agreement with other previously reported PM-OPD works, where the hole injection mechanism during illumination is described as tunneling.[17]

Another interesting finding here is that the barrier lowering effect due to IDIC is more dramatic compared to that of $PC_{71}BM$. For comparison, we conducted the same experiments, i.e., temperature-dependent *J-V* measurement for the $PC_{71}BM$-based PM-OPD. The results are summarized in Figure

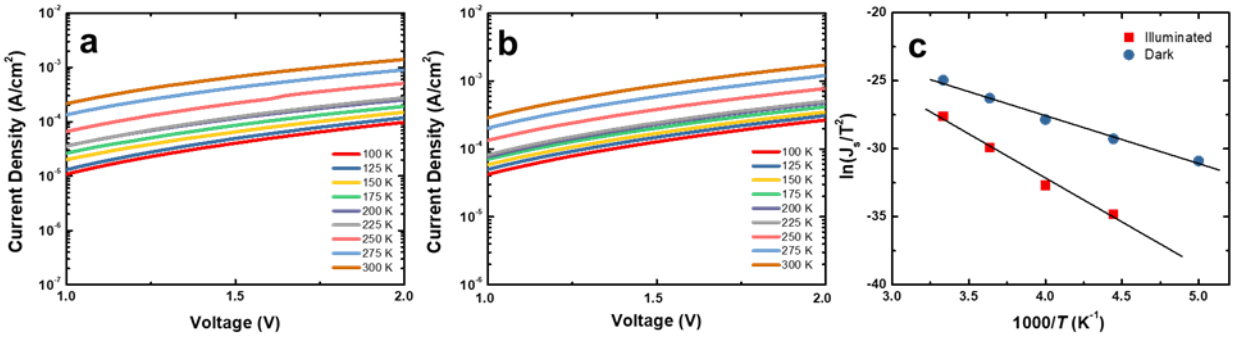

Figure 14. J-V characteristics of P3HT/PC71BM based PM-OPD under (a) dark and (b) light illumination (Power = 0.7419 mW/cm2, wavelength = 445 nm) at various temperatures in the forward bias regions. (c) Experimentally obtained ln (JsT−2) versus 1000/T plot under both dark and illuminated conditions to calculate the Schottky barrier height.

The extracted effective Schottky barrier height was 0.56 eV for dark condition, which is similar to the case of the PM-OPD with IDIC. However, the effective barrier decreased to only 0.30 eV, which is a significantly smaller decrease than the case with IDIC.

Collectively, these results indicate that by allowing more susceptible hole injection via tunneling through P3HT/Al Schottky barrier, IDIC can be a more efficient optical sensitizer in the PM-OPDs. This phenomenon can be attributed to energetically and spatially more confined nature of IDIC as an optical sensitizer.

Then, to demonstrate the PM-OPD performances of the P3HT/IDIC combination, we structured the device as ITO/PEDOT:PSS/P3HT/IDIC/Al while maintaining the active layer thickness as ~150 nm. This thickness was chosen for a comparative study against our earlier report on the $PC_{71}BM$-based PM-OPDs.[10]

As summarized in Figure 14(a), IDIC-based PM-OPD shows typical photoconductor *J-V* responses, i.e., despite high dark current originating from a thin active layer thickness (~150

nm), the photoconductive gain enables sufficiently higher photocurrent under a light intensity of 44.7 μW/cm^2 and wavelength of 450 nm. EQE was accordingly measured as shown in Figure 14(b) with a peak value over 130,000% at 380 nm and 600 nm under 19 V of reverse bias.

The reason why the EQE spectrum is not similar to the absorption spectrum of P3HT can be explained by different absorption mechanisms of photons with various absorption coefficients. For example, 550 nm wavelength photon—which corresponds to the maximum absorption of P3HT film—has the shortest penetration depth of ~61 nm within the active layer due to its extremely high absorption coefficient. In this case, a relatively large portion of photons cannot reach the charge separation region where IDIC molecules are spatially confined. Therefore, a relative EQE value at 550 nm should be smaller compared to the aspect of absorption spectrum. The obtained 130,000% EQE is higher than that of the $PC_{71}BM$-based PM-OPD with the same device architecture.[10] It is so far the highest value among all the PM-OPDs reported, implying that IDIC can be an ideal optical sensitizer for P3HT-based PM-OPDs.[8,9,10]

As an essential unit of image sensor technology, the most important figure-of-merit of PM-OPDs would be the specific detectivity (D^*), which is defined as

$$D^* = \frac{q\lambda G\sqrt{A}}{hci_n}$$

where λ is the illumination wavelength, G is the gain, A is the area of the active layer, h is the Planck's constant, c is the speed of light, and i_n is the noise current. To complete the D^* calculation, the noise current spectrum was obtained at 10 V of reverse bias and is summarized in Figure 3(c), which closely follows the shot noise limit.[18] Figure 14(d) shows the calculated

D*, which significantly exceeds 10^{12} Jones, and is higher than those of the state-of-the-art PCBM-based PM-OPDs.

Thus, we demonstrated the superiority of IDIC over $PC_{71}BM$ as an optical sensitizer of the PM-OPDs, which can be mainly attributed to more efficient charge trapping. The 2D planar IDIC molecular structure with inherently anisotropic packing structure is known to inhibit effective electron percolation pathway.[12] Therefore, we can possibly correlate the more efficient charge trapping behavior of IDIC not only from its deeper LUMO level but also its inherently anisotropic charge transport property.

This may enable further decrease of the active layer thickness of PM-OPDs, overcoming the lower thickness limit of this type of devices (which was due to electron percolation pathway formation within the thin active layer). Therefore, we tried to prepare 70-nm-thick PM-OPDs for the first time, with the assistance of IDIC as an optical sensitizer.

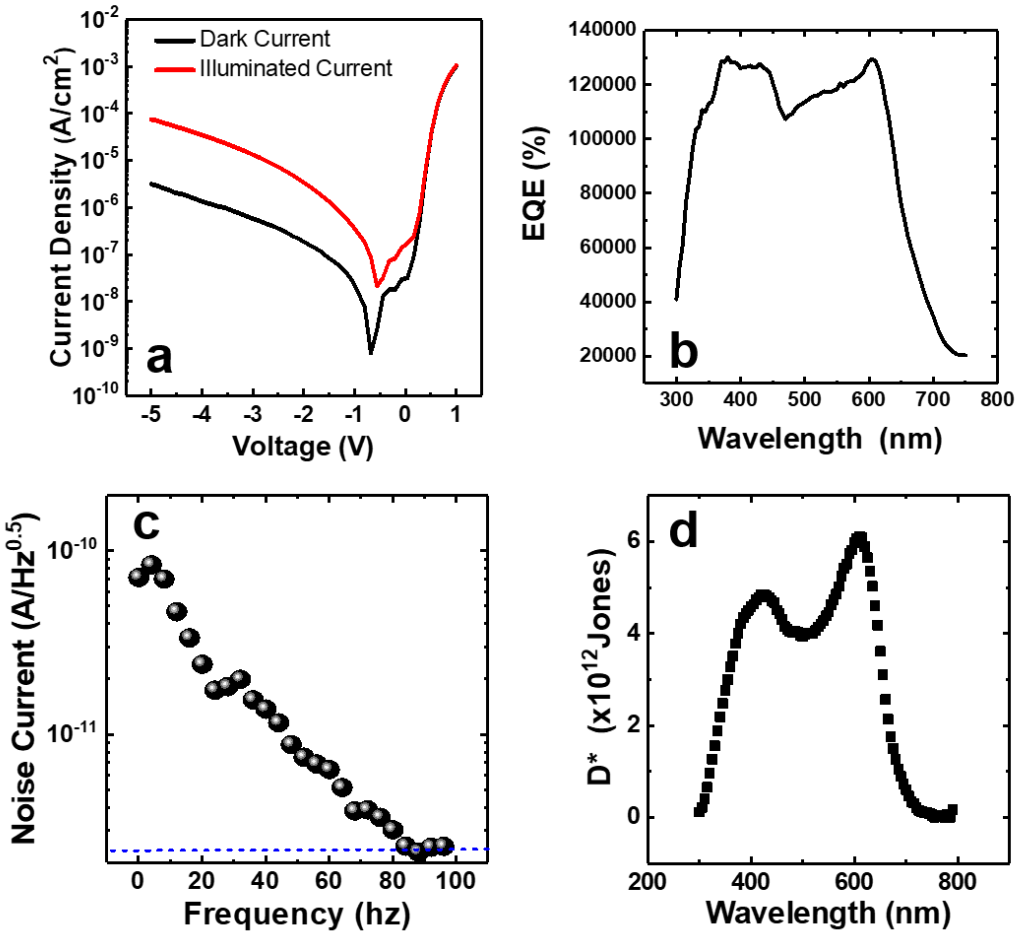

Figure 15. (a) J-V characteristics of PM-OPD with a 150-nm-thick active layer under dark and illuminated conditions (wavelength of 450 nm and power intensity of 44.7 μW/cm2), (b) EQE spectrum with a maximum of 130,000% measured at 19 V under reverse bias, (c) noise current spectrum measured at 10 V under reverse bias, and (d) the corresponding specific detectivity spectrum.

Figures 16(a) and (b) show the *J-V* characteristics and corresponding EQE spectrum, respectively, with the maximum EQE value of 60,700%, which is two times lower than that of the 150-nm-thick device. Theoretically, under a constant applied bias, $gain = \mu\tau V L^{-2}$[19]; therefore, a 70-nm-thick PM-OPD should have an EQE value approximately 4.5 times higher than that of the 150-nm-thick device. This implies that the 70-nm-thick active layer permits

some portion of the trapped electrons within the IDIC domains to escape to an external circuit that can reduce photoconductive gain.

Nonetheless, 60,700% of EQE is still noticeably higher than previously reported PM-OPDs.[8,9] The achieved active layer thickness of 70 nm is almost 7 times thinner as compared to the state-of-the-art OPD devices, which can dramatically accelerate the degree-of-integration of the photodiode as a unit pixel of the image sensor.

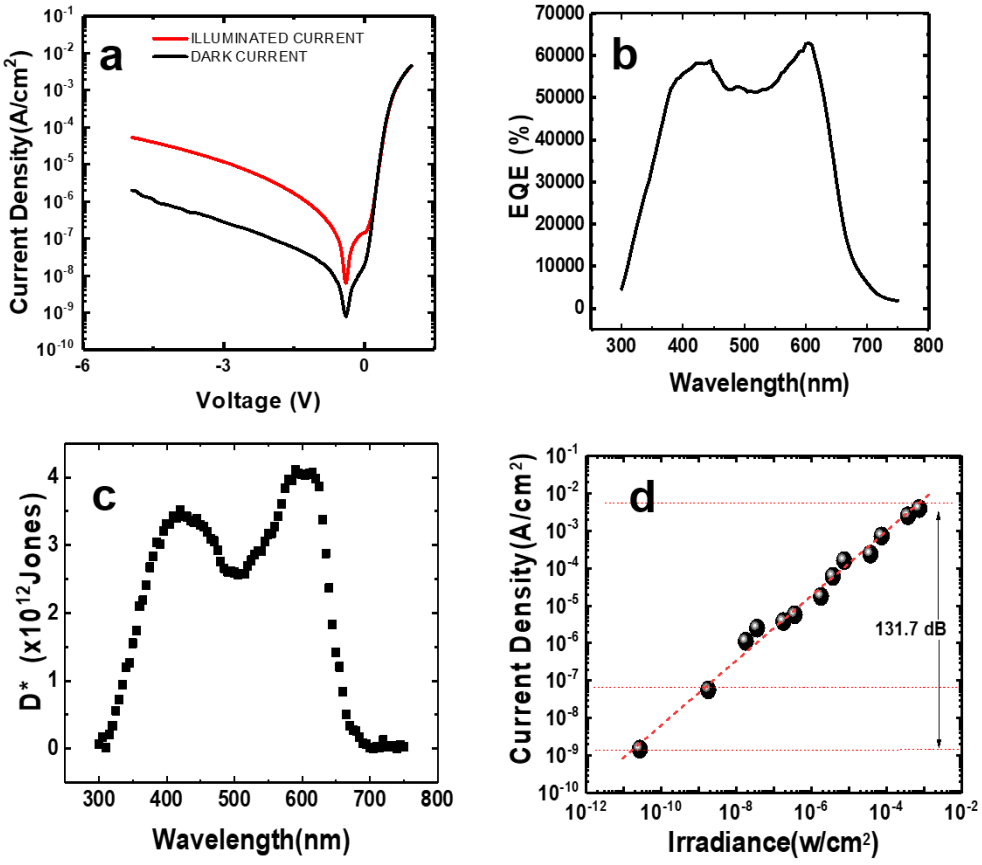

Figure 16. (a) J-V characteristics of PM-OPD with a 70-nm-thick active layer under dark and illuminated conditions (wavelength of 450 nm and power intensity of 39.81 μW/cm2), (b) EQE spectrum with a maximum of 60,700% measured at 19 V under reverse bias, (d) LDR range

Figure 16(c) shows the corresponding D* spectrum with a peak detectivity over 10^{12} Jones, which is sufficiently high for commercial application. The noise current spectrum used for the D* calculation is shown below. To further test the feasibility of the fabricated thin IDIC-based PM-OPD for commercial application, the linear dynamic range (LDR) of the suggested PM-OPD with an active layer thickness of 70 nm was measured. The LDR corresponds to the range where the power of the incident light and the intensity of the signal maintain a linear relationship, which is very important for the outdoor application of the image sensors.

In Figure 16(d), the photocurrent of the PM-OPD is plotted as a function of light intensity. Assuming that the noise-equivalent power of the fabricated PM-OPD can be regarded as the lower limit of LDR,[20] a high LDR value of 131.7 dB was obtained, which is the highest of all the reported high-performance PM-OPDs.

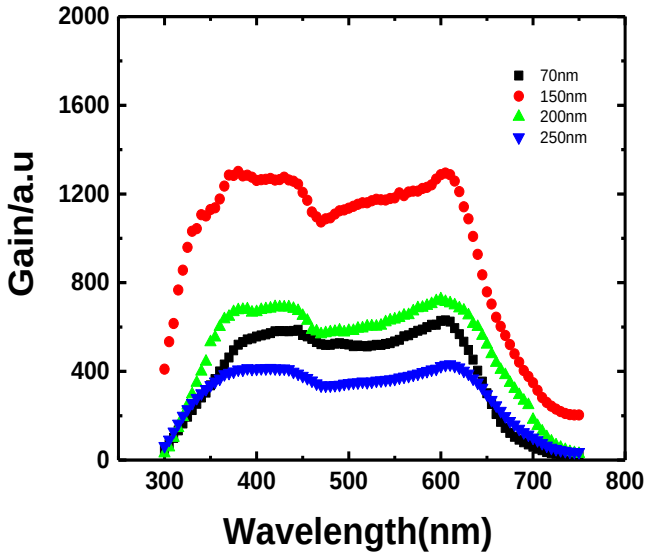

Figure 17. Comparison of Gain obtained by various thick active layer at -19 V

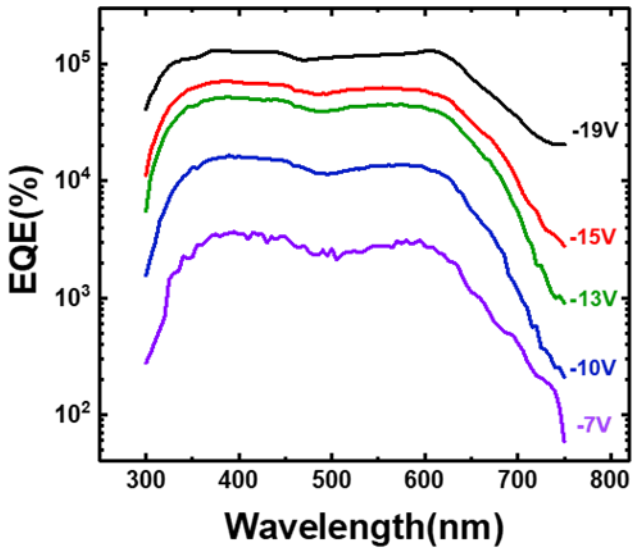

Figure 18. Comparison of EQE obtained by the 150nm thick photdetector under different reverse bias condition

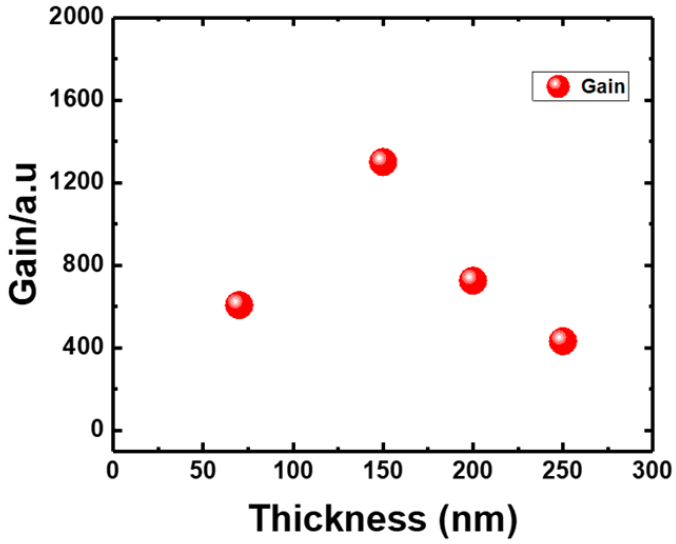

Figure 19. Maximum Gain obtained at different active layer thickness

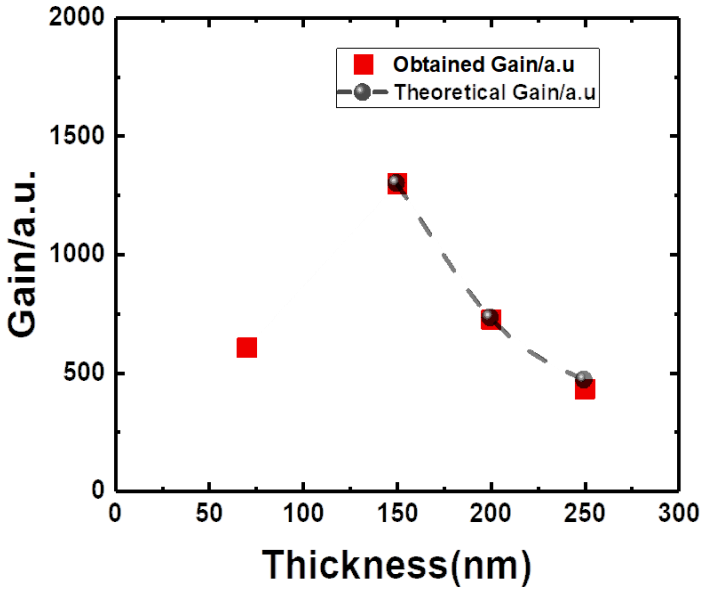

Figure 20. Theoretical Gain Vs Experimental Gain

ACTIVE LAYER THICKNESS (nm)	Maximum Obtained EQE (%)
250	43,100
200	72,500
150	130,000
70	60,700

Table 2. Thickness Vs Maximum EQE obtained

4. Conclusion

This paper suggests a new approach to achieve a high EQE along with a thinner active layer of PM-OPD. The introduction of a nonfullerene acceptor, IDIC, as an optical sensitizer—instead of the conventional $PC_{71}BM$—enabled more efficient Schottky–Ohmic tunable junction at P3HT/Al interface, as confirmed by the temperature-dependent *J-V* measurement assisted with diode equation analyses. This could be attributed to an energetically more favorable LUMO level of IDIC and also to its inherently less efficient charge percolation ability. As a result, the suggested PM-OPD structured as ITO/PEDOT:PSS/P3HT/IDIC/Al resulted in unprecedentedly high EQE over 130,000% with an active layer of 150 nm thickness. This EQE is much higher than the previous reports with $PC_{71}BM$ as an optical sensitizer. Furthermore, the unique advantage of IDIC as an optical sensitizer enabled further decrease of the active layer to 70 nm, while maintaining D* over 10^{12} Jones. This work opens the possibility of ultra-thin photodiode pixels, which can dramatically enhance the degree-of-integration of image sensors.

References

[1] Ahmadi, M.; Wu, T.; Hu, B. A Review on Organic–Inorganic Halide Perovskite Photodetectors: Device Engineering and Fundamental Physics. *Adv. Mater.* **2017**, *29*, 1605242.

[2] Sim, K. M.; Yoon, S.; Cho, J.; Jang, M. S.; Chung, D. S. Facile Tuning the Detection Spectrum of Organic Thin Film Photodiode via Selective Exciton Activation. *ACS Appl. Mater. Interfaces* **2018**, *10*, 8405-8410.

[3]https://news.panasonic.com/global/press/data/2018/02/en180214-2/en180214-2.html, (accessed January 2019).

[4] Armin, A.; Hambsch, M.; Kim, I. K.; Burn, P. L.; Meredith, P.; Namdas, E. B. Thick Junction Broadband Organic Photodiodes. *Laser Photonics Rev.* **2014**, *8*, 924-932.

[5] Yoon, S.; Jo, J. W.; Yu, S. H.; Yun, J. H.; Son, H. J.; Chung, D. S. Development of Novel Conjugated Polyelectrolytes as Water-Processable Interlayer Materials for High-Performance Organic Photodiodes, *ACS Photon.* **2017**, *4*, 703-709.

[6] Yoon, S.; Cho, J.; Sim, K. M.; Ha, J.; Chung, D. S. Low Dark Current Inverted Organic Photodiodes Using Anionic Polyelectrolyte as a Cathode Interlayer. *Appl. Phys. Lett.* **2017**, *110*, 083301.

[7] Pierre, A.; Deckman, I.; Lechêne, P. B.; Arias, A. C. High Detectivity All-Printed Organic Photodiodes. *Adv. Mater.* **2015**, *27*, 6411-6417.

[8] Kim, K., Sim, K. M., Yoon, S., Jang, M. S., Chung, D. S. Defect Restoration of Low-Temperature Sol-Gel-Derived ZnO via Sulfur Doping for Advancing Polymeric Schottky Photodiodes. *Adv. Funct. Mater.* **2018**, 28, 1802582

[9] Miao, J.; Zhang, F. Recent Progress on Photomultiplication Type Organic Photodetectors. *Laser & Photonics Reviews* **2019**, 13, 1800204.

[10] Li, L.; Zhang, F.; Wang, W.; An, Q.; Wang, J.; Sun, Q.; Zhang, M. Trap-Assisted Photomultiplication Polymer Photodetectors Obtaining an External Quantum Efficiency of 37 500%. *ACS Appl. Mater. Interfaces*. **2015**, *7*, 5890-5897.

[11] Wang, W.; Zhang, F.; Du, M.; Li, L.; Zhang, M.; Wang, K.; Wang, Y.; Hu, B.; Fang, Y.; Huang, J. Highly Narrowband Photomultiplication Type Organic Photodetectors. *Nano Lett.* **2017**, *17*, 1995-2002.

[12] Jang, M. S.; Yoon, S.; Sim, K. M.; Cho, J.; Chung, D. S. Spatial Confinement of the Optical Sensitizer to Realize a Thin Film Organic Photodetector with High Detectivity and Thermal Stability. *J. Phys. Chem. Lett.* **2018**, *9*, 8-12.

[13] Wang, W.; Du, M.; Zhang, M.; Miao, J.; Fang, Y.; Zhang, F. Organic Photodetectors with Gain and Broadband/Narrowband Response under Top/Bottom Illumination Conditions. *Adv. Opt. Mater.* **2018**, 6, 1800249.

[14] Miao, J. L.; Zhang, F. J.; Du, M. D.; Wang, W. B.; Fang, Y. Photomultiplication Type Organic Photodetectors with Broadband and Narrowband Response Ability. *Adv. Opt. Mater.* **2018**, 6, 1800001.

[15] Li, L.; Zhang, F.; Wang, W.; Fang, Y.; Huang, J. Revealing the Working Mechanism of Polymer Photodetectors with Ultra-High External Quantum Efficiency. *Phys. Chem. Chem. Phys.* ***2015****, 17*, 30712-30720.

[16] Yan, C.; Barlow, S.; Wang, Z.; Yan, H.; Jen, A. K. –Y.; Marder, S. R.; Zhan, X. Non-

Fullerene Acceptors for Organic Solar Cells. *Nat. Rev. Mater*. **2018**, *3*, 18003.

[17] Li, L.; Zhang, F.; Wang, J.; An, Q.; Sun, Q.; Wang, W.; Zhang, J.; Teng, F. Achieving EQE of 16,700% in P3HT: $PC_{71}BM$ Based Photodetectors by Trap-Assisted Photomultiplication. *Sci. Rep.* **2015**, *5*, 9181.

[18] Li, L.; Zhang, F.; An, Q.; Wang, Z.; Wang, J.; Tang, A.; Peng, H.; Xu, Z.; Wang, Y. Organic Ultraviolet Photodetector Based on Phosphorescent Material. *Opt. Lett.* **2013**, *38*, 3823-3826.

[19] Sze, S. M.; Ng, K. K. *Physics of semiconductor*, 3rd ed.; Wiley: New York, 2007, pp.722.

[20] Kang, W. P.; Davidson, J. L.; Gurbuz, Y.; Kerns, D. V. Temperature Dependence and Effect of Series Resistance on the Electrical Characteristics of a Polycrystalline Diamond Metal-Insulator-Semiconductor Diode. *J. Appl. Phys.* **1995**, *78*, 1101-1107.

[21] Dong, R.; Fang, Y.; Chae, J.; Dai, J.; Xiao, Z.; Dong, Q.; Yuan, Y.; Centrone, A.; Zeng, X. C.; Huang, J. High-Gain and Low-Driving-Voltage Photodetectors Based on Organolead Triiodide Perovskites. *Adv. Mater.* **2015**, *27*, 1912-1918.

[22] Armin, A.; Jansen-van Vuuren, R. D.; Kopidakis, N.; Burn, P. L.; Meredith, P. Narrowband Light Detection via Internal Quantum Efficiency Manipulation of Organic Photodiodes. *Nat. Commun.* **2015**, *6*, 6343.

[23] Gong, X.; Tong, M.; Xia, Y.; Cai, W.; Moon, J. S..; Cao, Y.; Yu, G.; Shieh, C. L.; Nilsson, B.; Heeger, A. J.; *Science* **2009**, 325, 1665−1667.

[24] Campbell, I. H.; Crone, B. K. Bulk Photoconductive Gain in Poly(Phenylene Vinylene) Based Diodes. *J. Appl. Phys.* **2007**, *101*, 024502.

[25] Lin, Q.; Armin, A.; Lyons, D. M.; Burn, P. L.; Meredith, P. Low Noise, IR-Blind Organohalide Perovskite Photodiodes for Visible Light Detection and Imaging. *Adv. Mater.* **2015**, *27*, 2060-2064.

[26] Chen, H. Y.; LoMichael, K. F.; Yang, G.; Monbouquette, H. G.; Yang, Y. Nanoparticle-assisted High Photoconductive Gain in Composites of Polymer and Fullerene. *Nat. Nanotechnol*. **2008**, 3, 543−547

[27] Chen, F. C.; Chien, S. C.; Cious, G. L. Highly Sensitive, Low voltage, Organic Photomultiple Photodetectors Exhibiting Broadband Response. *Appl. Phys. Lett.* **2010**, 97, 103301.

[28] Dong, R.; Bi, C.; Dong, Q.; Guo, F.; Yuan, Y.; Fang, Y.; Xiao, Z.; Huang, J. An Ultraviolet-to-NIR Broad Spectral Nanocomposite Photodetector with Gain. *Adv. Opt. Mater*. **2014**, 2, 549−554.

[29] Tan, W. C.; Shih, W. H.; Chen, Y. F. A Highly Sensitive Graphene-Organic Hybrid Photodetector with a Piezoelectric Substrate. *Adv. Funct. Mater*. **2014**, 24, 6818−6825

[30] Guo, F. W.; Yang, B.; Yuan, Y. B.; Xiao, Z. G.; Dong, Q. F.; Bi, Y.; Huang, J. S. A Nanocomposite Ultraviolet Photodetector Based on Interfacial Trap-Controlled Charge Injection. *Nat. Nanotechnol*. **2012**, 7, 798−802

[31] Chuang, S. T.; Chien, S. C.; Chen, F. C. Extended Spectral Response in Organic Photomultiple Photodetectors Using Multiple Near-Infrared Dopants. *Appl. Phys. Lett.* **2012**, 100, 013309

[32] Wang. W.; Zhang, F.; Li, L.; Zhang, M.; An, Q.; Wang, J.; Sun, Q. Highly Sensitive

Polymer Photodetectors with a Broad Spectral Response Range from UV Light to the Near Infrared Region. *J. Mater. Chem. C* **2015**, 3, 7386

[33] Miao, J.; Zhang, F.; Lin, Y.; Wang, W.; Gao, M.; Li, L.; Zhang, J.; Zhan, X. Highly Sensitive Organic Photodetectors with Tunable Spectral Response under Bi-Directional Bias. *Adv. Opt. Mater*. **2016**, 4, 1711.

[34] Shen, L.; Fang, Y.; Wei, Y.; Yuan, Y.; Huang, J. A Highly Sensitive Narrowband Nanocomposite Photodetector with Gain. *Adv. Mater.* **2016**, 28, 2043

[35] Christopher, W, R.; Scott, A. M.; Adam J. M. Investigating the Morphology of Polymer/Fullerene Layers Coated Using Orthogonal Solvents. *J. Phys. Chem. C* **2012**, 116, 13, 7287-7292

[36] Lin, Y.; He, Q.; Zhao, F.; Huo, L.; Mai, J.; Lu, X.; Su, C. J.; Li, T.; Wang, J.; Zhu; , J.; Sun, Y.; Wang, C.; Zhan, X. A Facile Planar Fused-Ring Electron Acceptor for As-Cast Polymer Solar Cells with 8.71% Efficiency. J. Am. Chem. Soc. 2016, 138, 2973−2976.

요 약 문

용액전이 광 증감 제로 비 풀러렌 기반 2D 평면형 소분자 반도체를

본 논문은 ...

본 연구에서는 100 nm 이하의 얇은 광활성층 두께 조건에서 높은 외부 양자 효율을 구현하기 위해, 평면 분자 구조를 가지는 비 풀러렌 전자 받개인 2,2′ -((2Z,2′ Z)-((4,4,9,9-tetrahexyl-4,9-dihydro-s-indaceno[1,2-b:5,6-b′]dithiophene-2,7-diyl)bis(methanylylidene))bis(3-oxo-2,3-dihydro-1H-indene-2,1-diylidene))dimalononitrile (IDIC)의 광학적 감응제(optical sensitizer)로서의 활용 가능성을 타진하였다. 본 연구는 핵심은 기존의 구형 구조를 가지는 풀러렌 계열 전자 받개(PC61BM, PC71BM)에서 보이는 등방적인 전자 전달과는 반대인 IDIC 의 비등방적인 전자 전달을 활용하는 것으로, 이러한 비등방적인 패킹 구조는 전자의 효율적인 여과 경로(percolation pathway)의 형성을 저해하게 된다. 따라서 이러한 현상은 전하의 트랩에 있어 굉장히 용이하다고 할 수 있는데, 때문에 광 증폭(photomultiplication) 메커니즘 기반의 유기 포토디텍터(organic photodetector, OPD) 구조에서 광학적 감응제로 적용하기에 적합하다고 할 수 있다. 또한, IDIC 는 기존의 풀러렌 계열 전자 받개들에 비해 가시광선 영역의 파장에 대해 더 높은 흡광 계수를 가지는데, 이는 흡광 효율의 향상을 야기하여, 결과적으로 기존에 비해 더 높은 광전류를 구현할 수 있게 한다. 상기 서술한 광물리적인 특성과 더불어, IDIC 는 풀러렌 계열 전자 받개에 비해 더 낮은 최저 빈 분자 궤도(lowest unoccupied molecular orbital, LUMO) 준위를 가지는데, 이러한 특성 또한 PM-OPD 구조에서 광학적 감응제로서 풀러렌 계열 전자 받개에 비해 더욱 낫다고 할 수 있다. 소자 구현을 위해, 광활성층으로 IDIC 와 함께 poly(3-hexylthiophene-2,5-diyl) (P3HT)을 사용하였고, 소자 성능의 비교를 위해 IDIC 대신 PC71BM 을 적용한 소자 또한 제작하였다. 더 효율적인 광 증폭 메커니즘 구현을 위해, P3HT 와 IDIC 또는 PC71BM 을 층층이 배치(layer-by-layer deposition)하였고, 이를 통해 약 150 nm 의 매우 얇은 광활성층을 이용하여 130,000% 이상의 외부 양자 효율과 1012 Jones 이상의 검출능을 가지는 고성능 유기 포토디텍터를 구현할 수 있었다. 또한, 기존 풀러렌 계열 전자 받개를 사용한 경우에 비해 IDIC 를 사용할 때 더 강한 전하의 공간적 구속(spatial confinement)이 이루어짐을 확인하여 광활성층의 두께를 더욱 낮추었고, 약 70 nm 정도의 매우 얇은 광활성층 조건에서도 60,000% 이상의 매우 높은 외부 양자 효율을 보임을 확인하였다.

핵심어: 사진 곱셈, 광 검출기, 고감도, 광학 증감 기

ACKNOWLEDGEMENT

Even though words aren't enough to express my gratitude, I wholeheartedly would thank to my supervisor, Prof. Dae Sung Chung, for the great guidance and taking care of me throughout these last two years.

I also like to thank all the PEML laboratory lab mates for providing the motivations and emotional supports that I needed.